1989

Mechanism of Collisionally-Induced Transitions Among Fine-Structure Levels: Semiclassical Calculations of Alignment Effects in the Na-He System

Laurie J. Kovalenko

Stephen R. Leone

John B. Delos
William & Mary, jbdelo@wm.edu

Recommended Citation

Kovalenko, Laurie J.; Leone, Stephen R.; and Delos, John B., Mechanism of Collisionally-Induced Transitions Among Fine-Structure Levels: Semiclassical Calculations of Alignment Effects in the Na-He System (1989). *Journal of Chemical Physics*, 91(11), 6948-6960.
https://doi.org/10.1063/1.457312

Mechanism of collisionally induced transitions among fine-structure levels: Semiclassical calculations of alignment effects in the Na–He system

Laurie J. Kovalenko and Stephen R. Leone[a)]
Joint Institute for Laboratory Astrophysics, University of Colorado and National Institute of Standards and Technology, and Department of Chemistry and Biochemistry, University of Colorado, Boulder, Colorado 80309-0440

John B. Delos[b)]
Physics Department, College of William and Mary, Williamsburg, Virginia 23185

(Received 10 April 1989; accepted 15 August 1989)

To gain insight into the mechanism of $Na(3p)^2P_{3/2} \rightarrow {}^2P_{1/2}$ fine-structure transitions induced by collision with He, we monitor the expectation values of the orbital- and spin-angular momentum vectors, **l** and **s**, as a function of time along the trajectory, using a semiclassical formalism. In a typical collision, $\langle \mathbf{s} \rangle$ remains nearly space-fixed while $\langle \mathbf{l} \rangle$ precesses about the rotating internuclear axis. Thus, in the interaction region, the projection of $\langle \mathbf{l} \rangle$ onto the internuclear axis, $\langle \lambda \rangle$, remains nearly constant, and the molecular alignment of the orbital is preserved. We show how equations of motion for the classical analogues of these expectation values agree qualitatively with the quantum equations of motion. A qualitative comparison is also made with the Cs–He system for which the spin–orbit coupling is much stronger. We calculate cross sections for $Na(^2P_{3/2}) + He \rightarrow Na(^2P_{1/2}) + He$ as a function of the alignment of the excitation laser polarization with respect to the asymptotic relative velocity vector. For stationary pumping of the excited $F = 3$ hyperfine level, this calculation predicts that the perpendicular alignment gives a cross section which is larger by a factor of 1.8 than that obtained by parallel alignment.

I. INTRODUCTION

Collisionally induced transitions among fine-structure levels have been extensively studied, but more can be learned, especially in regard to alignment and orientation effects and the mechanisms of the transfer. One of the simplest cases is the process

$$Na(3p\,^2P_{3/2}) + He \rightarrow Na(3p\,^2P_{1/2}) + He\,. \qquad (1.1)$$

A complete and rigorous theory of these processes involves calculation of the full quantum wave function $\psi(\mathbf{R},\mathbf{r})$ describing the motion of the nuclei and of the active electron. This "close-coupling" theory begins with an expansion of the wave function in molecular electronic states, and ends with numerical solution of coupled equations for nuclear wave functions and numerical summation over coupled angular momentum states. For process (1.1) (and others) this theory has been implemented by Reid,[1] Pascale and Olson,[2] and Lemoine, Robbe, and Pouilly,[3] and it is known to give accurate cross sections. However the formulation of the theory and the long numerical codes are very complex and physical insight can be lost.

A more intuitive, though less rigorous, semiclassical model has successfully been used to treat these systems. Nikitin[4] used a strong coupling approximation to obtain analytic formulas for the fine-structure transition cross sections in the Na–Ar system. Masnou-Seeuws,[5] with Roueff[6] numerically solved more exact equations for the Na–He system using a semiclassical impact parameter method; this calculation was later refined by Masnou-Seeuws and McCarroll[7] to take into account trajectory effects. More recently, Schmidt, Bähring, and Witte[8] emphasized the importance of including the spin–orbit interaction for electronic energy transfer in collisions of Na* with Na^+.

The main goal of the present work is to obtain an understanding of the mechanism of fine-structure transitions. In particular, we study the Na–He system for which the relevant potential energy curves are known.[9] Using a semiclassical model, we monitor expectation values of the electronic orbital- and spin-angular momentum vectors, $\langle \mathbf{l} \rangle$ and $\langle \mathbf{s} \rangle$, as functions of time along the trajectory. The behavior of these vectors can be interpreted in very simple ways. Also, we give equations of motion for the classical analogs of these expectation values, and we show that they agree qualitatively with the quantum equations of motion. We then compare the Na–He system to the Cs–He system, where the spin–orbit coupling is much stronger.

As a consequence of our analysis, we provide a new level of understanding of the concept of orbital locking.[8,10,11] This concept is very old. In the context of collision processes like (1.1), orbital locking and related ideas can be found implicitly in Refs. 4–7; however, in the context of molecular structure theory, related ideas can be traced back to the work of Hund[12] in the 1920's and 1930's. Therefore, it may seem surprising that these concepts are presently objects of controversy. Pouilly and Alexander[13] have strongly challenged the concept of orbital locking, saying "Perhaps the concept of a *locking radius* should better be replaced by that of a *scrambling radius*, inside of which it is impossible, quantum

[a)] Staff Member, Quantum Physics Division, National Institute of Standards and Technology.
[b)] 1986–87 JILA Visiting Fellow.

 0021-9606/89/236948-13$02.10

mechanically, to specify the orientation of the p orbital." Their work illustrates very well the fact that accurate quantum calculations are possible, but an intuitive picture that is consistent with such calculations is still lacking. Part of the purpose of this paper is to provide such an intuitive picture. The accompanying full-quantum calculation by Schatz, Kovalenko, and Loene[14] confirms many aspects of our calculations, and directly addresses problems in the interpretation given in Ref. 13.

In addition to our qualitative results, we calculate the experimentally measurable alignment ratio, $\sigma_{\|}/\sigma_{\perp}$, for Na fine-structure transitions induced by collision with He. We model a crossed beam experiment in which the Na atom is excited by a linearly polarized laser propagating perpendicular to both atomic beams. The effect of the alignment of the laser polarization vector with respect to the initial average relative velocity vector has been measured for electronic energy transfer in other systems: the alkaline earth atoms Ca[15] and Sr,[16] and Ne**.[17] The Ca experiment has been studied theoretically by Devdariani and Zagrebin[18] using a semiclassical method, and by Pouilly and Alexander[19] using a full quantum method. The Ne** experiment has also been studied with both semiclassical[20] and full quantum methods.[21] In all these experiments, the integral cross section is measured. In this paper we also calculate integral cross sections. A review of more detailed crossed beam experiments which measure differential cross sections is given in Campbell, Schmidt, and Hertel.[22]

We first calculate the Na–He alignment ratio for the hypothetical case that Na has no hyperfine structure. Our result agrees well with a subsequent full quantum calculation presented in the accompanying paper.[14] We then repeat the calculation, this time for stationary pumping[23] of the $F=3$ hyperfine level. This alignment ratio has not yet been measured experimentally. As a check on our calculation, we compute the total degeneracy averaged cross section and compare it to both experiment[24] and previous theory.[1,7]

We mention an aspect of our notation. The quantum operator corresponding to, for example, the electronic orbital angular momentum vector is $\mathbf{l}$ (boldface); the matrix representing this operator is l and its expectation value is $\langle \mathbf{l} \rangle$ (bracketed). The classical dynamical variable corresponding to this quantum operator is $\bar{\mathbf{l}}$ (overlined). The space-fixed coordinate system, x', y', z', is distinguished from the rotating molecular coordinate system, x, y, z, by primes.

II. THEORY

Our approach is a modification of that developed by Masnou-Seeuws and McCarroll.[7] The Na^*–He system is regarded as a three-particle system consisting of a He atom, a Na^+ core, and an active electron. The motions of He and of the Na^+ core are described by classical mechanics, while the motion of the active electron is described by quantum mechanics.[25] Trajectories are generated such that total energy and total angular momentum are conserved (nuclear kinetic energy plus expectation value of electronic energy equals a constant; the same holds true for angular momentum).

A. Schrödinger equation for the electron

Let $\mathbf{r}$ be the vector representing the position of the active electron relative to the Na^+ core, and let $\mathbf{R}=\mathbf{R}(t)$ be the internuclear vector, pointing from He to Na^+. The length and direction of $\mathbf{R}$ are given by polar coordinates $[R(t),\Theta(t),\Phi(t)]$ defined in the laboratory relative to the asymptotic relative velocity vector. The Hamiltonian for the active electron is

$$h[\mathbf{r};\mathbf{R}(t)] = h_{\rm el}[\mathbf{r};\mathbf{R}(t)] + h_{\rm soc}\ , \tag{2.1}$$

where $h_{\rm el}[\mathbf{r};\mathbf{R}(t)]$ is the electrostatic part of the Hamiltonian (also called the "Born–Oppenheimer Hamiltonian"),

$$h_{\rm el}[\mathbf{r},\mathbf{R}(t)] = -\frac{\hbar^2}{2m}\nabla_r^2 + V_{e^-,{\rm Na}^+}(\mathbf{r}) + V_{e^-,{\rm He}}[\mathbf{r};\mathbf{R}(t)]\ , \tag{2.2}$$

where m is the electron mass and $h_{\rm soc}$ is the spin–orbit term[26]

$$h_{\rm soc} = \xi(r)\mathbf{l}\cdot\mathbf{s}\ . \tag{2.3}$$

The wave function Ψ, including spatial and spin variables, satisfies a time-dependent Schrödinger equation

$$h\Psi = i\hbar\partial\Psi/\partial t. \tag{2.4}$$

The Schrödinger equation is reduced to a set of coupled equations by expansion in a basis[27]

$$\Psi = \sum_k c_k(t)\phi_k[\mathbf{r};\mathbf{R}(t)]\ , \tag{2.5}$$

$$i\hbar\frac{d}{dt}\mathsf{c}(t) = \{\mathsf{h}[\mathbf{R}(t)] + \mathbf{v}(t)\cdot\mathsf{P}[\mathbf{R}(t)]\}\mathsf{c}(t)\ . \tag{2.6}$$

Here $\mathsf{h}[\mathbf{R}(t)]$ is the matrix representing the Hamiltonian (2.1),

$$h_{jk}[\mathbf{R}(t)] = \langle\phi_j|h[\mathbf{r};\mathbf{R}(t)]|\phi_k\rangle\ , \tag{2.7a}$$

and it is the sum of electrostatic and spin–orbit terms

$$\mathsf{h}[\mathbf{R}(t)] = \mathsf{h}_{\rm el}[\mathbf{R}(t)] + \mathsf{h}_{\rm soc}\ . \tag{2.7b}$$

$\mathbf{v}(t)$ is the relative nuclear velocity, and

$$\mathbf{v}\cdot\mathbf{P}_{jk}[\mathbf{R}(t)] = \mathbf{v}\cdot\langle\phi_j| - i\hbar\nabla_{\mathbf{R}}\phi_k\rangle\ , \tag{2.7c}$$

represents the total rate-of-change of the basis functions with the (vectorial) internuclear separation; i.e., it is the matrix representing nonadiabatic coupling.[28] (It arises because we use basis functions that rotate with the internuclear axis.)

B. Born–Oppenheimer basis

The elements of the matrices h and P depend upon the basis functions $[\phi_k(\mathbf{r};\mathbf{R})]$ that are chosen. Several choices are possible. We choose the "Born–Oppenheimer" basis, in which the states are eigenfunctions of $h_{\rm el}(\mathbf{r};\mathbf{R})$:

$$h_{\rm el}(\mathbf{r};\mathbf{R})\phi_k(\mathbf{r};\mathbf{R}) = \epsilon_k(R)\phi_k(\mathbf{r};\mathbf{R})\ . \tag{2.8}$$

The basis was truncated to the set of six states that correlates at large R to the $3p$ configuration of Na. These states can be labeled by two quantum numbers, λ and σ, which are the components of electronic orbital and spin angular momentum about the internuclear axis. At large distances R, these states become eigenfunctions of the isolated Na atom Hamiltonian (excluding spin-orbit coupling)

$$\phi_k(\mathbf{r};\mathbf{R}) \equiv \phi_{\lambda\sigma}(\mathbf{r};\mathbf{R}) \overset{R\to\infty}{\to} W(r)\,Y_{l\lambda}(\theta,\phi)|\sigma\rangle \leftrightarrow W(r)|l\lambda s\sigma\rangle\,, \tag{2.9}$$

where $W(r)$ is the radial electronic wave function for the Na $3p$ states and $Y_{l\lambda}(\theta,\phi)$ is the spherical harmonic ($l=1$) defined relative to the internuclear axis. Likewise $|\sigma\rangle$ is the spin ket ($\sigma = \pm 1/2$) also defined relative to that axis. (Phase conventions on angular momentum eigenstates are those of Condon and Shortley[26]; the direction from He to Na is the positive z axis.)

The eigenvalues $\epsilon_k(R)$ were computed by Pascale,[9,29] and we fit his numerical results to analytical formulas. We should mention that the usual instinct is to fit the eigenvalues most accurately at small distances ($R \sim 1 - 5a_0$), where the forces are largest. However, in the present case it is most important to fit the eigenvalues accurately at larger distances ($R \sim 8 - 17a_0$). It is in this region that the competition between the three terms $\mathsf{h}_{el}(\mathbf{R})$, h_{soc} and $\mathbf{v}\cdot\mathsf{P}(\mathbf{R})$ determines the transition probabilities. Moreover, we chose to fit the sum and difference potentials, since the transition probability is mainly determined by the latter. Our formulas are (in atomic units)

$$\begin{aligned}\epsilon_{sum} &= \epsilon_\Sigma + \epsilon_\Pi \\ &= -(3.566\times10^{-4})e^{-0.23425R} \\ &\quad + 2.790e^{-0.7711R} - 25.16\left[\frac{R-2.039}{R^2}\right]e^{-0.85R}, \\ \epsilon_{diff} &= \epsilon_\Sigma - \epsilon_\Pi \\ &= 1.3547e^{-0.6972R} \\ &\quad - 7.336\left[\frac{R+0.25}{5.25}\right]e^{-1.14R}.\end{aligned} \tag{2.10}$$

ϵ_{sum} is related to the spherically averaged isotropic interaction between the active electron and He, while ϵ_{diff} is related to the anisotropy of this interaction. This anisotropy causes electronic (j,m_j) transitions. The electronic energy curves $\epsilon_\Sigma(R)$ and $\epsilon_\Pi(R)$ are shown in Fig. 1.

To calculate the matrix elements of h_{soc} and $\mathsf{P}(\mathbf{R})$ we note that again we need accurate values mainly at large $R(8a_0 \lesssim R \lesssim 18a_0)$ where these matrix elements are comparable to $\epsilon_\Sigma - \epsilon_\Pi$. The wave functions given in Eq. (2.9), which are exact as $R\to\infty$, should be sufficiently accurate in this range of R to meet our needs.

Calculation of spin–orbit matrix elements in the Born–Oppenheimer representation is then a familiar exercise. All of these matrix elements are proportional to the value of an integral,[26] ζ, whose magnitude is determined from the spin–orbit splitting in isolated Na($3p$) atoms[30]:

$$\Delta E = \tfrac{3}{2}\zeta = 17.20\ \text{cm}^{-1},$$

so $\zeta = 11.46\ \text{cm}^{-1}$. The spin-orbit Hamiltonian matrix is then

$$\mathsf{h}_{soc} = \zeta\mathbf{l}\cdot\mathbf{s}\,. \tag{2.11}$$

Within the approximations used here, this matrix is independent of internuclear separation.

The nonadiabatic coupling matrix $\mathsf{P}(\mathbf{R})$ consists of radial and angular parts:

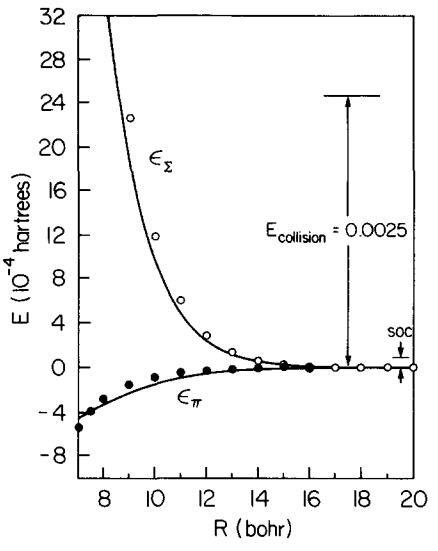

FIG. 1. Electronic energy curves for Na($3p$) and He, without spin–orbit coupling. Curves are fits to values calculated by Pascale: $\epsilon_\Pi(R)$, $\epsilon_\Sigma(R)$. The average collision energy and the atomic spin–orbit splitting are indicated.

$$\mathbf{v}\cdot\mathsf{P} = \frac{dR}{dt}P^R + \frac{d\theta}{dt}P^\theta + \frac{d\phi}{dt}P^\phi = \dot{R}P^R + \dot{\theta}P^\theta + \dot{\phi}P^\theta\,. \tag{2.12}$$

In the truncated Born–Oppenheimer representation used here, all matrix elements of P^R ("radial coupling" elements) vanish,

$$P^R_{jk} \equiv \langle\phi_j| - i\hbar\frac{\partial}{\partial R}|\phi_k\rangle = 0\,, \tag{2.13}$$

because the states ϕ_j, ϕ_k have different angular symmetry (different values of λ or σ).

Angular couplings follow from the formula[27]

$$\dot{\theta}\mathsf{P}^\theta + \dot{\phi}\mathsf{P}^\phi = -\dot{\theta}\mathsf{j}_y + \dot{\phi}(\mathsf{j}_z\cos\theta + \mathsf{j}_x\sin\theta)\,, \tag{2.14}$$

where $\mathbf{j} = \mathbf{l} + \mathbf{s}$ is the operator representing total electronic angular momentum.

The full 6×6 Hamiltonian matrix is given in Fig. 2.

The advantage of this representation is that the largest matrix elements [$\epsilon_\Sigma(R)$ and $\epsilon_\Pi(R)$] are diagonal; this makes numerical integration more efficient. However, the basis states in this representation do not correspond to initial or final states; those would be space-fixed atomic states, eigenfunctions of $h_{el} + h_{soc}$ for the isolated Na atom. Rotating (body-fixed) atomic states are characterized by quantum numbers $|lsj\Omega\rangle$, and they are related to the Born–Oppenheimer states $|l\lambda s\sigma\rangle$ by Clebsch–Gordan coefficients.[26] Space-fixed atomic states are related to rotating atomic states by d matrices.[31]

C. Nuclear trajectory

Trajectories which conserve total energy and angular momentum can be derived from the equations of motion[32]

$$\frac{d\mathbf{R}}{dt} = \mathbf{v}\,, \tag{2.15a}$$

l_z, s_z	1, +1/2	1, -1/2	0, +1/2	0, -1/2	-1, +1/2	-1, -1/2
1, +1/2	$\epsilon_\pi + \frac{\zeta}{2} - \frac{3A}{2}$	$\frac{B}{2}$	$\frac{B}{\sqrt{2}}$			
1, -1/2	$\frac{B^*}{2}$	$\epsilon_\pi - \frac{\zeta}{2} - \frac{A}{2}$	$\frac{\zeta}{\sqrt{2}}$	$\frac{B}{\sqrt{2}}$		
0, +1/2	$\frac{B^*}{\sqrt{2}}$	$\frac{\zeta}{\sqrt{2}}$	$\epsilon_\Sigma - \frac{A}{2}$	$\frac{B}{2}$	$\frac{B}{\sqrt{2}}$	
0, -1/2		$\frac{B^*}{\sqrt{2}}$	$\frac{B^*}{2}$	$\epsilon_\Sigma + \frac{A}{2}$	$\frac{\zeta}{\sqrt{2}}$	$\frac{B}{\sqrt{2}}$
-1, +1/2			$\frac{B^*}{\sqrt{2}}$	$\frac{\zeta}{\sqrt{2}}$	$\epsilon_\pi - \frac{\zeta}{2} + \frac{A}{2}$	$\frac{B}{2}$
-1, -1/2				$\frac{B^*}{\sqrt{2}}$	$\frac{B^*}{2}$	$\epsilon_\pi + \frac{\zeta}{2} + \frac{3A}{2}$

FIG. 2. The full 6×6 Hamiltonian matrix using the Born–Oppenheimer representation. Basis functions are labeled $|\lambda,\sigma\rangle$. ϵ_Π, and ϵ_Σ are eigenvalues of the electronic Hamiltonian. ζ is related to the spin–orbit coupling term and is equal to 5.2×10^{-5} a.u. A and B are related to the angular coupling terms and are equal to $\dot\phi\cos(\Theta)$, and $\dot\phi\sin(\Theta) + i\dot\Theta$, respectively.

$$\frac{\mu d\mathbf{v}}{dt} = -\langle \nabla_{\mathbf{R}} h[\mathbf{r};\mathbf{R}(t)]\rangle$$
$$= -\mathbf{c}^\dagger(t)\nabla\mathbf{h}[\mathbf{R}(t)]\mathbf{c}(t)\,, \tag{2.15b}$$

where the matrix $\nabla\mathbf{h}[\mathbf{R}(t)]$ has elements[33] $\langle\phi_j|\{\nabla_{\mathbf{R}} h[\mathbf{r};\mathbf{R}(t)]\}|\phi_k\rangle$, and μ is the reduced mass of the nuclei. Equation (2.15) has the following physical meaning: The force between He and Na depends upon whether the electron is in the Σ or the Π state; since the electronic wave function is generally a linear combination of Σ and Π states, we calculate an average force $\langle\nabla_{\mathbf{R}} h(\mathbf{r};\mathbf{R})\rangle$ using the appropriate weighting factors, which are the amplitudes $\mathbf{c}(t)$.

From Eqs. (2.15) it is not hard to show that total energy

$$E = \mu\mathbf{v}^2/2 + \langle h[\mathbf{r};\mathbf{R}(t)]\rangle \tag{2.16}$$

and total angular momentum

$$\mathbf{J} = \mathbf{N} + \langle\mathbf{j}\rangle \tag{2.17}$$

are constants of the motion. (Here $\mathbf{N}$ is the relative angular momentum of the nuclei, which has initial magnitude equal to μvb.) Using the well-known formulas

$$N_z = \mu R^2\dot\phi\sin^2\theta\,, \tag{2.18a}$$
$$\mathbf{N}^2 = \mu^2R^4(\dot\theta^2 + \dot\phi^2\sin^2\theta)\,, \tag{2.18b}$$

equations for the nuclear trajectory can be derived

$$\frac{dR}{dt} = v_R\,, \tag{2.19a}$$
$$\frac{\mu dv_R}{dt} = \left\langle -\frac{\partial h}{\partial R}\right\rangle + \frac{\mathbf{N}^2}{\mu R^3}\,, \tag{2.19b}$$
$$\frac{d\theta}{dt} = (\mathbf{N}^2 - N_z^2/\sin^2\theta)^{1/2}/\mu R^2\,, \tag{2.19c}$$
$$\frac{d\phi}{dt} = N_z/\mu R^2\sin^2\theta\,. \tag{2.19d}$$

These four equations of nuclear motion (2.19) are integrated simultaneously with the six coupled equations for the electron motion (2.6). At each step in time, expectation values $\langle(\partial/\partial R)h[\mathbf{r};\mathbf{R}(t)]\rangle$ and $\langle\mathbf{j}\rangle$ are computed, and $\mathbf{N}$ is evaluated using Eq. (2.17) (taking into account the intial value of $\mathbf{J}$); hence time derivatives of R, v_R, θ and ϕ are determined.[34]

III. PICTURES OF THE EVOLUTION OF ELECTRONIC ANGULAR MOMENTA

The theory described above is known to give a reasonably accurate description of typical fine-structure transitions.[7] To get a complete picture of the collision process, one could for each impact parameter examine the trajectory generated from Eqs. (2.6) and (2.19), and then examine the six complex amplitudes $c_k(t)$ as functions of time on this trajectory. However, it is hard to learn very much this way (Fig. 3).

A simpler picture of the collision process can be obtained by monitoring expectation values of the electronic angular momentum vectors $\langle\mathbf{l}\rangle$, $\langle\mathbf{s}\rangle$, and $\langle\mathbf{j}\rangle$ as functions of time along a trajectory. Each element of these vectors is given by an expectation value, such as

$$\langle l_x\rangle = \mathbf{c}^\dagger(t)\mathbf{l}_x\mathbf{c}(t) \tag{3.1}$$

where $\mathbf{l}_x$ is the matrix representing the component of the electronic angular momentum operator along the rotating x axis in the Born–Oppenheimer basis. Using the approximate wave functions, Eq. (2.9), these matrices are easy to derive, and their expectation values can be computed at regular time steps along the trajectory. Equation (3.1) gives the components of these vectors in the rotating molecular frame of reference (z along the internuclear axis). Two Euler rotations using the angles $\Theta(t)$, $\Phi(t)$ (which specify the instantaneous orientation of the internuclar axis) are then used to give the components of $\langle\mathbf{l}\rangle$, $\langle\mathbf{s}\rangle$, and $\langle\mathbf{j}\rangle$ in the space-fixed frame.

In most of the calculations for these pictures we used a moderately large impact parameter ($b = 10\,a_0$). We chose initial conditions $c_k(t_0)$ so that we could easily see the time-evolution of $\langle\mathbf{l}\rangle$, $\langle\mathbf{s}\rangle$, and $\langle\mathbf{j}\rangle$. (Our initial conditions do not

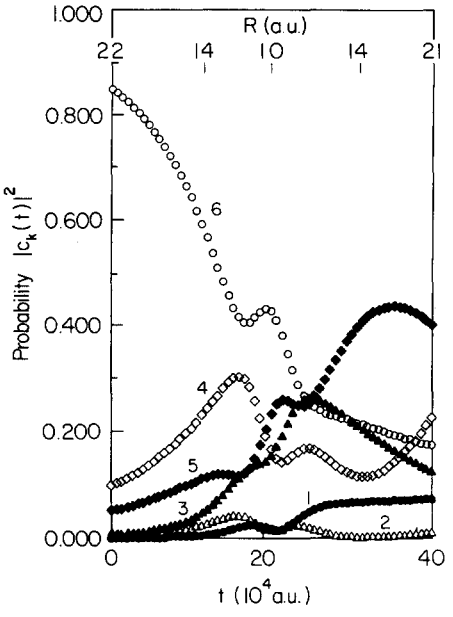

FIG. 3. Probability, $|c_k(t)|^2$, for being in each basis state, $|\lambda,\sigma\rangle$, as a function of time along a trajectory. (A few correspnding values of R are given above the figure; note that R is not a linear function of time.) Basis functions are in order: $|1,1/2\rangle,|1,-1/2\rangle,|0,1/2\rangle,|0,-1/2\rangle,|-1,1/2\rangle,|-1,-1/2\rangle$. This particular trajectory corresponds to the initial state $|j,m_j'\rangle = |3/2,3/2\rangle$, $v = 0.0009$ a.u., and an impact parameter of 10 a.u. If the graph were extended to even earlier times, $|c_6(t)|^2$ would approach 1. At such early times, the quantization axis for the molecular frame, z, is opposite to the quantization axis of the space-fixed frame, z'. Hence the initial state is equivalently expressed as $|m_l' = 1,m_s' = 1/2\rangle$ or $|\lambda = -1,\sigma = -1/2\rangle$.

necessarily correspond to any easily attained experimental situation.) We emphasize that the drawings in this section depict the actual time evolution of the system, as computed by the method described in Sec. II.

The exact evolution of the angular momentum vectors is complicated, because it is determined by the relative magnitudes of three competing effects: the electrostatic fields of He, spin–orbit coupling in Na, and the rotation of the internuclear axis over the course of the collision. First, it is easiest to examine these effects one at a time by setting some of the parameters equal to zero.

A. Electrostatic coupling only

Let us set the spin–orbit coupling constant ζ to zero, and freeze the motion of the nuclei by setting $\dot{R} = \dot{\Theta} = \dot{\Phi} = 0$. Initial conditions on the amplitudes $c_k(t)$ are arbitrary, and we take care only so that $\langle \mathbf{l} \rangle$ and $\langle \mathbf{s} \rangle$ do not initially vanish, and are not initially collinear. Then integration of (2.6) with fixed nuclei leads to the result that $\langle \mathbf{l} \rangle$ precesses about the internuclear axis, while $\langle \mathbf{s} \rangle$ remains space-fixed [Fig. 4(a)]. Thus the expectation value of the projection of $\mathbf{l}$ onto the internuclear axis, $\langle l_z \rangle = \langle \lambda \rangle$, is conserved. Somewhat surprisingly, $\langle \mathbf{l} \rangle$ traces out not a circle, but an elliptical cone; the angular frequency for precession is $\omega_{el} = (\epsilon_\Sigma - \epsilon_\Pi)/\hbar$. The anisotropy of the electrostatic interaction of the electron with He couples the electronic orbital angular momentum to the internuclear axis.

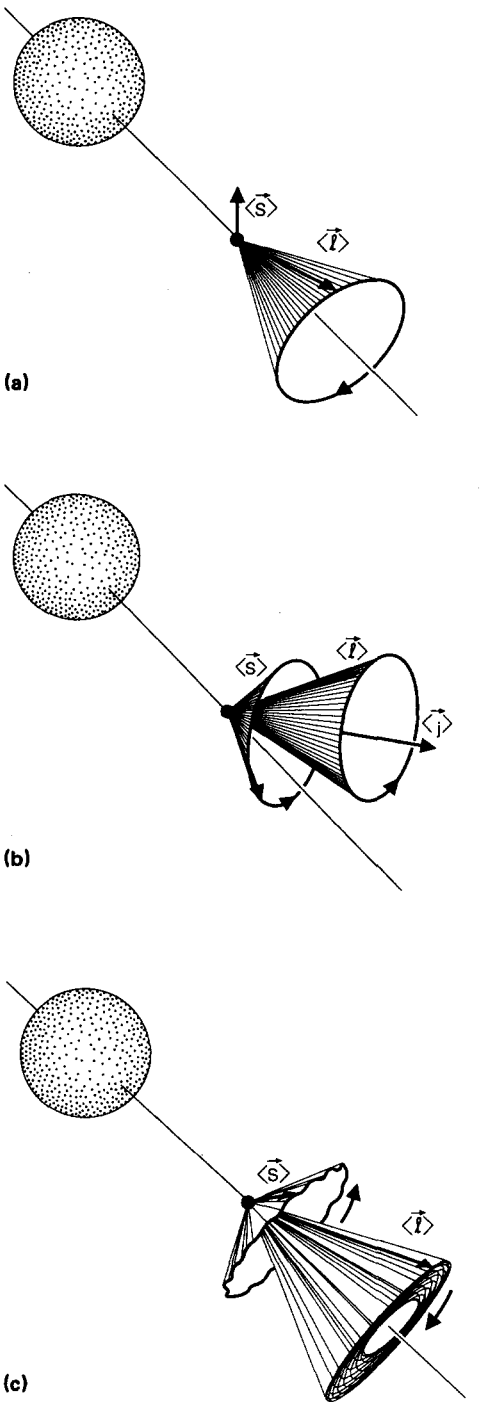

FIG. 4. (a) Influence of the anisotropy of the electrostatic interaction, $\Delta\epsilon_{\Pi,\Sigma}$, between the He and the Na. The spin–orbit interaction and the angular coupling terms in the Hamiltonian have been set to zero. The He atom is represented by the ball at the upper left, the Na by its electronic orbital- and spin-angular momentum vectors, $\langle \mathbf{l} \rangle$ and $\langle \mathbf{s} \rangle$. We see that $\langle \mathbf{l} \rangle$ precesses about the internuclear axis while $\langle \mathbf{s} \rangle$ remains space-fixed. $\langle \lambda \rangle$ is conserved. Thus the anisotropy of the electrostatic interaction couples $\mathbf{l}$ to the internuclear axis, leaving $\mathbf{s}$ unaffected. (b) Influence of the spin–orbit interaction term on the electron. The anisotropy of the electrostatic interaction and the angular coupling terms in the Hamiltonian have been set to zero. We see that both $\langle \mathbf{l} \rangle$ and $\langle \mathbf{s} \rangle$ precess about each other; their sum, $\langle \mathbf{l} \rangle + \langle \mathbf{s} \rangle$, is a constant vector, $\langle \mathbf{j} \rangle$. Thus the spin–orbit interaction couples $\mathbf{l}$ and $\mathbf{s}$ to each other. (c) Anisotropy of electrostatic interaction $\gg$ spin–orbit interaction. The angular coupling terms in the Hamiltonian have been set to zero; however, the anisotropy of the electrostatic interaction term has been reinstated. We see that $\langle \mathbf{l} \rangle$ precesses rapidly about the internuclear axis while $\langle \mathbf{s} \rangle$ precesses much more slowly about $\langle \mathbf{l} \rangle$. Both $\langle \lambda \rangle$ and $\langle \sigma \rangle$ are conserved to a good approximation; their sum, $\langle \Omega \rangle$, is exactly conserved.

B. Spin–orbit coupling only

Again freezing the nuclear motion, we now set ϵ_{diff} to zero. This eliminates the anisotropy of the electrostatic interaction, thereby eliminating the electrostatic torque on the active electron. We reinstate the spin–orbit coupling by using the correct value of ζ. We find that $\langle \mathbf{l} \rangle$ and $\langle \mathbf{s} \rangle$ precess about each other at an angular frequency of $\omega_{\text{soc}} = (3/2)\zeta/\hbar$, and there is no coupling of $\langle \mathbf{l} \rangle$ to the internuclear axis. The cones traced out by $\langle \mathbf{l} \rangle$ and $\langle \mathbf{s} \rangle$ are approximately, but not exactly, concentric about $\langle \mathbf{j} \rangle$, which is conserved [Fig. 4(b)]. In this case too, the cones are elliptical.

C. Electrostatic and spin–orbit coupling

Still keeping the motion of the nuclei fixed, we now examine nonvanishing values of ϵ_{diff} and ζ. Two limiting cases arise:

1. Spin–orbit interaction ≪ anisotropy of electrostatic interaction

The orbital angular momentum $\langle \mathbf{l} \rangle$ precesses rapidly about the internuclear axis, while $\langle \mathbf{s} \rangle$ precesses much more slowly about the rapidly moving $\langle \mathbf{l} \rangle$ [Fig. 4(c)]. This behavior of $\langle \mathbf{l} \rangle$ differs from that shown in Fig. 4(a) in that the elliptical cone traced out by $\langle \mathbf{l} \rangle$ itself precesses and changes its eccentricity due to the influence of spin–orbit coupling. The behavior of $\langle \mathbf{s} \rangle$ differs from that shown in Fig. 4(b) in that the cone traced out by $\langle \mathbf{s} \rangle$ is scalloped due to the influence of electrostatic coupling; each scallop corresponds to one precession of $\langle \mathbf{l} \rangle$ about the internuclear axis. Note that the sense of precession of $\langle \mathbf{s} \rangle$ is opposite to that of $\langle \mathbf{l} \rangle$. The expectation value of the projection of both l and s onto the internuclear axis, $\langle \lambda \rangle$ and $\langle \sigma \rangle$, are nearly conserved, while their sum, $\langle \Omega \rangle$ is exactly conserved. (Here ζ was taken to be 11.46 cm^{-1}, which is its value for the Na atom, and $R = 10$ a.u.)

2. Anisotropy of electrostatic interaction ≪ spin–orbit interaction

Orbital and spin angular momenta precess rapidly about each other. Their resultant $\langle \mathbf{j} \rangle = \langle \mathbf{l} \rangle + \langle \mathbf{s} \rangle$ precesses slowly about the internuclear axis; $\langle \Omega \rangle$ is conserved [same behavior as in Fig. 4(b) except now $\langle \mathbf{j} \rangle$ traces a cone about the internuclear axis; its projection on that axis, $\langle \Omega \rangle$, remains constant]. (Here we took $\zeta = 369.2\ \text{cm}^{-1}$ which is its value for the Cs atom; $R = 10$ a.u.)

D. Angular coupling only

We now set the nuclei into motion, and set ζ and ϵ_{diff} to zero. The coupled equations contain only the angular coupling terms (2.14). The result is that $\langle \mathbf{l} \rangle$ and $\langle \mathbf{s} \rangle$ stay space-fixed, as if the He were not there at all. Angular couplings decouple the angular momenta from the internuclear axis.[35]

E. All couplings together

With all couplings included, the behavior of $\langle \mathbf{l} \rangle$ and $\langle \mathbf{s} \rangle$ depends upon the relative magnitudes of the three terms. These relative magnitudes change through the course of the collision. We now describe the sequence of events that is characteristic of Na*–He collisions at $b \sim 10\ a_0$, $v = 9 \times 10^{-4}$ a.u. ($\sim 2000\ \text{ms}^{-1}$) (kinetic energy = 0.0685 eV). To simplify the picture (Fig. 5) we use a straight line trajectory (the same initial conditions run with a 3-D trajectory resulted in a scattering angle of only 14° and an out-of-plane displacement of 2.5° over the course of the trajectory; the qualitative behavior of the electronic wave function was unaffected). The figure shows several snapshots of $\langle \mathbf{l} \rangle$ and $\langle \mathbf{s} \rangle$ over the course of the trajectory, projected onto the $x'z'$ collision plane (a) and the $z'y'$ plane (b).

(i) $R \sim \infty$: electrostatic coupling vanishes and the internuclear axis is fixed. Spin–orbit coupling dominates, so $\langle \mathbf{l} \rangle$ and $\langle \mathbf{s} \rangle$ precess slowly about each other; their resultant $\langle \mathbf{j} \rangle$ remains constant (Hund's case e).

(ii) $20 > R > 16$: Electrostatic coupling is still negligible. The internuclear axis is rotating, but the time required for the nuclei to move this distance is much less than the spin–orbit precession time. Angular couplings dominate, so $\langle \mathbf{l} \rangle$ and $\langle \mathbf{s} \rangle$ stay nearly space-fixed (Hund's case d).

(iii) $16 > R > 3$: Electrostatic coupling increases rapidly as R decreases, and over a distance of about $2\ a_0$ (between $16\ a_0$ and $14\ a_0$) it overwhelms spin–orbit coupling. In about the same range the electrostatic coupling also overwhelms the angular coupling. (Note that angular coupling depends upon the impact parameter and the initial velocity.) Hence $\langle \mathbf{l} \rangle$ begins precessing rapidly about the internuclear axis, and as the axis rotates the cone

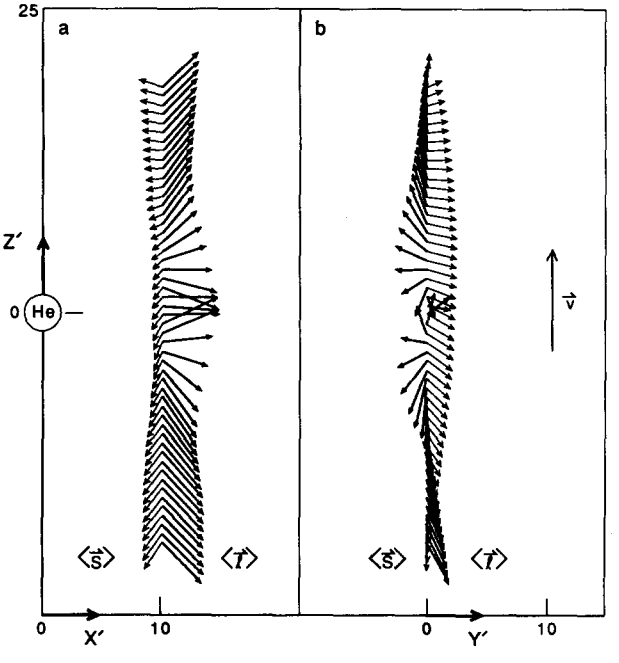

FIG. 5. A tyical trajectory. He is located at the origin of the space-fixed coordinate system. The Na atom is traveling in the direction of v. (a) shows projections of $\langle \mathbf{l} \rangle$ and $\langle \mathbf{s} \rangle$ onto the $x'z'$ collision plane and (b) onto the $y'z'$ plane. The motion of $\langle \mathbf{l} \rangle$ is seen to undergo one precession about the internuclear axis; during this same time $\langle \mathbf{s} \rangle$ rotates by only ~90°. This results in an overall change in the relative orientation of the two vectors, and thus a change in $\langle \mathbf{j} \rangle$. Therefore a fine structure transition has taken place.

traced out by $\langle \mathbf{l} \rangle$ follows it. (For $b = 10$ we see one precession over the course of the collision while for $b = 8$ there are about 5.) Let us use the phrase "l-locking" to refer to this type of motion. The spin, $\langle \mathbf{s} \rangle$, stays nearly space-fixed because the collision time is much less than the spin–orbit precession time (Hund's case b).

The collision partners pass through these regions on both the incoming and outgoing parts of the collision (Fig. 5). (Trajectories with other values of impact parameter give similar behavior.)

In the Na*–He system $jm_j \rightarrow j'm_j'$ transitions occur by the following mechanism. Suppose the system begins in the $j = 3/2$ state, in which $\langle \mathbf{l} \rangle$ and $\langle \mathbf{s} \rangle$ are aligned with each other. Then as a result of the collision, $\langle \mathbf{s} \rangle$ stays nearly space-fixed while the orientation of $\langle \mathbf{l} \rangle$ is changed. It follows that both the magnitude and the direction of $\langle \mathbf{j} \rangle$ are also changed by the collision. Change of orientation of $\langle \mathbf{j} \rangle$ corresponds to $m_j \rightarrow m_j'$ transitions. Usually a change of the magnitude of $\langle \mathbf{j} \rangle$ represents $j \rightarrow j'$ transitions. However, we must be a little cautious with this last statement: actually it is change of $\langle \mathbf{j}^2 \rangle$ that corresponds to $j \rightarrow j'$ transitions; since $\langle \mathbf{j}^2 \rangle \neq \langle \mathbf{j} \rangle^2$, it is sometimes possible for the magnitude of $\langle \mathbf{j} \rangle$ to change even when $\langle \mathbf{j}^2 \rangle$ does not change.

Now we examine the sequence of events characteristic of Cs*–He collisions at comparable impact parameters and somewhat lower relative velocities. We expect the Born–Oppenheimer energy curves for this system to be qualitatively similar to those of the Na*–He system. The important difference is that the spin–orbit coupling constant is 32 times larger for Cs*–He than for Na*–He. For simplicity, we use the same energy curves, and take $\zeta = 369.2\ \text{cm}^{-1}$, $b = 10\ a_0$, and $v = 500\ \text{ms}^{-1}$.

We find the following sequence of events:

(i) $\infty > R > 16\ a_0$: Spin–orbit coupling dominates. $\langle \mathbf{l} \rangle$ and $\langle \mathbf{s} \rangle$ precess rapidly about each other; their resultant $\langle \mathbf{j} \rangle$ remains space-fixed because angular couplings dominate over electrostatic couplings (Hund's case e, as in Fig. 5).

(ii) $16 > R > 9\ a_0$: Electrostatic coupling increases as R decreases. It dominates over angular couplings but remains small compared to spin–orbit coupling. $\langle \mathbf{j} \rangle$ begins to precess about the (rotating) internuclear axis (Hund's case c).

In this collision, the magnitude of $\langle \mathbf{j} \rangle$ stays approximately constant, but its orientation is changed by the collision. Hence $j \rightarrow j'$ transitions are improbable, but $m_j \rightarrow m_j'$ transitions have a large cross section.

If the impact parameter is smaller, then j-changing transitions will again occur. Consider a collision with $b \sim 5\ a_0$. As the atoms approach each other, they pass through regions (i) (case e) and (ii) (case c) as before. Then:

(iii) $8\ a_0 > R$: Electrostatic coupling dominates over spin–orbit coupling, and both of these dominate over angular coupling. Hence, as in Fig. 4(c), $\langle \mathbf{l} \rangle$ precesses rapidly about the internuclear axis, and $\langle \mathbf{s} \rangle$ precesses more slowly about the rapidly moving $\langle \mathbf{l} \rangle$ so both are locked onto the internuclear axis, but $\langle \mathbf{j} \rangle$ is not conserved (Hund's case a).

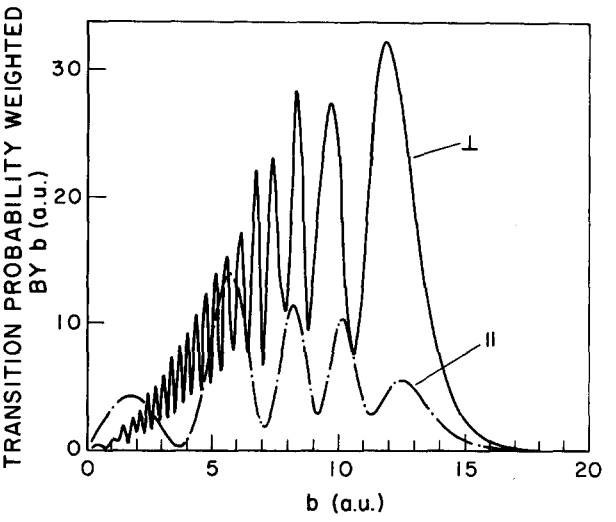

FIG. 6. Transition probabilities weighted by impact parameter vs. impact parameter. The dotted line is the integrand of $\sigma_{\parallel}$: $2\pi b P(b;\Theta_E = 0)$. The solid line is the integrand of $\sigma_{\perp}$: $\pi b[P(b;\Theta_E = \pi/2,\phi_E = 0) + P(b;\Theta_E = \pi/2,\phi_E = \pi/2)]$. The oscillations correspond to how much $\langle \mathbf{l} \rangle$ has precessed. For instance, minima result from trajectories where $\langle \mathbf{l} \rangle$ undergoes approximately an integral number of precessions.

This situation is similar to that for Na*–He except in one respect: in Na*–He the spin is nearly space-fixed, but in Cs*–He it precesses about the internuclear axis.

IV. EQUATIONS OF MOTION FOR $\langle \mathbf{l} \rangle$, $\langle \mathbf{s} \rangle$, AND $\langle \mathbf{j} \rangle$

All of the above pictures follow from direct solution to the coupled Eqs. (2.6) and (2.19), by monitoring expectation values of $\mathbf{l}$ and $\mathbf{s}$ as functions of time. Let us now consider an alternative approach. We would like to obtain equations of motion for $\langle \mathbf{l} \rangle$ and $\langle \mathbf{s} \rangle$—equations that give the rates of change of $\langle \mathbf{l} \rangle$ and $\langle \mathbf{s} \rangle$ in terms of their values at each instant throughout the collision.

In Sec. IV A we seek *quasiclassical* equations motion for $\langle \mathbf{l} \rangle$ and $\langle \mathbf{s} \rangle$—equations that can be written in Poisson-bracket form with an effective classical Hamiltonian. This classical Hamiltonian will be a smooth function of classical dynamical variables of the system, but it will be constructed from quantum information about the system. Specifically we shall use the Born–Oppenhiemer eigenvalues $\epsilon_k(R)$ and the spin–orbit coupling constant ζ to construct this classical Hamiltonian.[36,37] In Sec. IV B we will see how this quasiclassical treatment differs from the correct quantum mechanical treatment.

A. Quasiclassical equations of motion

1. The effective classical Hamiltonian

We begin from the matrix representation of the quantum Hamiltonian (2.7b), (2.8), and (2.11),

$$\mathsf{h} = \mathsf{h}_{\text{el}}(R) + \zeta\, \mathsf{l}\cdot\mathsf{s}\,. \tag{4.1}$$

The spin–orbit term carries over directly from quantum mechanics to classical mechanics. Let $\bar{\mathbf{l}}$, $\bar{\mathbf{s}}$ be *classical* orbital- and spin-angular-momentum vectors for the electron. Then the classical analogue of the spin–orbit matrix $\zeta\, \mathsf{l}\cdot\mathsf{s}$ is (obviously) the function $\zeta \bar{l}\cdot\bar{s}$.

Problem: How do we convert the matrix of Born–Oppenheimer eigenvalues $h_{el}(R)$ into a classical Hamiltonian function? The numerical value of the classical electrostatic Hamiltonian function must be equal to the electrostatic energy of the system at each internuclear separation. The quantum energy levels depend upon $\lambda = |\langle l_z \rangle|/\hbar$ (and parametrically upon R), so we expect that we can write a classical Hamiltonian $\bar{h}_{el}$ as a function of $\bar{l}_z$ and R: $\bar{h}_{el}(\bar{l}_z;R)$.

When $\bar{l}_z = \pm\lambda\hbar$, we take the classical Hamiltonian to be equal to the energy-eigenvalue corresponding to that vlaue of λ:

$$\bar{h}_{el}(\pm\lambda\hbar;R) = \epsilon_\lambda(R) . \tag{4.2}$$

The symmetry implicit in this equation suggests that the classical Hamiltonian should be a symmetric function of $\bar{l}_z$. For intermediate values of $\bar{l}_z$, the classical Hamiltonian should smoothly interpolate between the eigenvalues. In principle, any smooth interpolation is acceptable; we use a polynomial. If there are $l+1$ distinct eigenvalues $\epsilon_\lambda(R)$ of h_{el}, then we may take $\bar{h}_{el}(\bar{l}_z;R)$ to be an l^{th} degree polynomial in $(\bar{l}_z)^2$, having coefficients $p_m(R)$ that depend smoothly upon R

$$\bar{h}_{el}(\bar{l}_z;R) = \sum_{m=0}^{l} p_m(R)(\bar{l}_z)^{2m} . \tag{4.3}$$

In the present case, $l=1$ so

$$\bar{h}_{el}(\bar{l}_z;R) = \epsilon_\Sigma(R) + [\epsilon_\Pi(R) - \epsilon_\Sigma(R)](\bar{l}_z)^2 . \tag{4.4}$$

Finally, we note that $\bar{l}_z$ represents the component of the orbital angular momentum about the rotating internuclear axis,

$$\bar{l}_z = \hat{\mathbf{R}}(t)\cdot\bar{\mathbf{l}} , \tag{4.5}$$

where $\bar{\mathbf{l}}$ is the classical angular momentum, and $\hat{\mathbf{R}}(t)$ is the unit vector along the internuclear axis (from He to Na).

We therefore write the full classical Hamiltonian function $\bar{h}(\bar{\mathbf{l}},\bar{\mathbf{s}};\mathbf{R})$ in the form

$$\bar{h}(\bar{\mathbf{l}},\bar{\mathbf{s}};\mathbf{R}) = \bar{h}_{el}(\hat{\mathbf{R}}(t)\cdot\bar{\mathbf{l}};R) + \zeta\,\bar{\mathbf{l}}\cdot\bar{\mathbf{s}} . \tag{4.6}$$

2. Evolution of angular momentum vectors

Classical equations of motion can now be derived easily using the Poisson-bracket formalism. If $(\bar{l}_{x'},\bar{l}_{y'},\bar{l}_{z'})$ refer to classical components of the angular momentum vector along space-fixed axes (x',y',z'), then the important brackets are

$$[\bar{l}_{x'},\bar{l}_{y'}] = \bar{l}_{z'} , \tag{4.7a}$$

and cyclic permutations thereof; also

$$[\bar{l}_f,\bar{s}_f] = 0, \tag{4.7b}$$

$$[\bar{l}_i, f(\bar{l}_f)] = \partial f(\bar{l}_f)/\partial\bar{l}_f\,[\bar{l}_i,\bar{l}_f] . \tag{4.7c}$$

[Here $f(l_f)$ is any differentiable function.]

From these formulas one can derive

$$[\bar{\mathbf{l}},\bar{\mathbf{l}}\cdot\bar{\mathbf{s}}] = \bar{\mathbf{s}}\times\bar{\mathbf{l}} , \tag{4.8a}$$

$$[\bar{\mathbf{s}},\bar{\mathbf{l}}\cdot\bar{\mathbf{s}}] = \bar{\mathbf{l}}\times\bar{\mathbf{s}} , \tag{4.8b}$$

$$[\bar{\mathbf{l}},(\hat{\mathbf{R}}\cdot\bar{\mathbf{l}})^{2m}] = 2m(\hat{\mathbf{R}}\cdot\bar{\mathbf{l}})^{2m-1}\,\hat{\mathbf{R}}\times\bar{\mathbf{l}} . \tag{4.8c}$$

It follows that equations of motion for $\bar{\mathbf{s}}$ and $\bar{\mathbf{l}}$ are

$$\frac{d\bar{\mathbf{s}}}{dt} = \zeta\bar{\mathbf{l}}\times\bar{\mathbf{s}} , \tag{4.9a}$$

$$\frac{d\bar{\mathbf{l}}}{dt} = [\mathbf{G}(\bar{l}_z;\mathbf{R}) + \zeta\,\bar{\mathbf{s}}]\times\bar{\mathbf{l}} , \tag{4.9b}$$

where

$$\mathbf{G}(\bar{l}_z;\mathbf{R}) = \hat{\mathbf{R}}\frac{\partial\bar{h}_{el}(\bar{l}_z;R)}{\partial\bar{l}_z} . \tag{4.9c}$$

$\mathbf{G}(\bar{l}_z;\mathbf{R})$ is a vector that lies along the (rotating) internuclear axis. Its magnitude, $|\partial\bar{h}_{el}(\bar{l}_z;R)/\partial\bar{l}_z|$, changes with time as R and $\bar{l}_z$ vary. The vector $\mathbf{G}(\bar{l}_z;\mathbf{R})$ points from the collision partner to the atom with the active electron whenever $\partial\bar{h}_{el}(\bar{l}_z;R)/\partial\bar{l}_z$ is positive, and it points in the opposite sense whenever this quantity is negative. The specific polynomial interpolation (4.4) gives

$$\mathbf{G}(\bar{l}_z;\mathbf{R}) = 2[\epsilon_\Pi(R) - \epsilon_\Sigma(R)]\bar{l}_z\hat{\mathbf{R}}(t) . \tag{4.10}$$

We note that $\mathbf{G}(\bar{l}_z;\mathbf{R})$ is an antisymmetric function of $\bar{l}_z$; $\mathbf{G}(\bar{l}_z;\mathbf{R})$ points from Na to He when $\bar{l}_z$ is positive and in the opposite sense when $\bar{l}_z$ is negative.

These equations of motion (4.9) describe the evolution of the vectors $\bar{\mathbf{l}}(t),\bar{\mathbf{s}}(t)$. By examining various limiting cases, we can see that these vectors have behavior simlar to that of the expectation values $\langle\mathbf{l}\rangle$, $\langle\mathbf{s}\rangle$, as discussed in Sec. III.

For example, if $\mathbf{G}(\bar{l}_z;\mathbf{R}) = 0$, then the equations of motion can be written in the form (with $\bar{\mathbf{j}} = \bar{\mathbf{l}} + \bar{\mathbf{s}}$)

$$\frac{d\bar{\mathbf{l}}}{dt} = \zeta(\bar{\mathbf{j}}\times\bar{\mathbf{l}}) , \tag{4.11a}$$

$$\frac{d\bar{\mathbf{s}}}{dt} = \zeta(\bar{\mathbf{j}}\times\bar{\mathbf{s}}) , \tag{4.11b}$$

$$\frac{d\bar{\mathbf{j}}}{dt} = 0 , \tag{4.11c}$$

so $\bar{\mathbf{l}}$ and $\bar{\mathbf{s}}$ precess about the conserved $\bar{\mathbf{j}}$. For ζ positive ("normal" order of spin–orbit levels, characteristic of atoms on the left-hand-side of the periodic table), the precession is in a right-handed sense (right thumb along $\bar{\mathbf{j}}$, fingers curl in direction of motion of $\bar{\mathbf{l}}$ and $\bar{\mathbf{s}}$).

On the other hand, if $\zeta = 0$, then the equations of motion are

$$\frac{d\bar{\mathbf{s}}}{dt} = 0 , \tag{4.12a}$$

$$\frac{d\bar{\mathbf{l}}}{dt} = \mathbf{G}(\bar{l}_z;\mathbf{R})\times\bar{\mathbf{l}} . \tag{4.12b}$$

Hence $\bar{\mathbf{s}}$ is space-fixed, and $\bar{\mathbf{l}}$ precesses in a right-hand sense about $\mathbf{G}(\bar{l}_z;\mathbf{R})$, which itself rotates with the internuclear axis, varies in magnitude, and may even change its sense as the collision proceeds. If the precession is rapid compared to the rotation of $\mathbf{G}$, then the cone traced out by $\bar{\mathbf{l}}$ locks onto the rotating axis. It is also interesting to note that if $\bar{\mathbf{l}}$ is perpendicular to $\mathbf{R}$, so $\bar{l}_z = 0$, then $\mathbf{G} = 0$, and at that instant, this classical treatment predicts that precession stops.

These quasiclassical equations enable us to predict the sense of precession of the vectors without any calculation (see figures).

B. Quantum effects

The quasiclassical equations of motion derived and discussed in the preceding section provide a helpful intuitive

picture of the evolution of the angular momentum vectors during a collision. In this section we ask what differences exist between the behavior of the classical quantities and the behavior of the quantum expectation values.

Quantum expectation values satisfy the equation of motion

$$\frac{d}{dt}\langle F\rangle = (i\hbar)^{-1}\langle [F,h]\rangle + \left\langle \frac{\partial F}{\partial t}\right\rangle \tag{4.13}$$

where F is any dynamical variable, and now $[F,h]$ is the commutator of F with the electronic Hamiltonian. It is easy to show that the equations of motion for the quantum expectation values of the spin- and orbital-angular momentum vectors are:

$$\frac{d}{dt}\langle \mathbf{s}\rangle = \zeta\langle \mathbf{l}\times\mathbf{s}\rangle ,$$

$$\frac{d}{dt}\langle \mathbf{l}\rangle = \frac{1}{i\hbar}\langle [\mathbf{l},h_{el}(l_z;R)]\rangle + \zeta\langle \mathbf{s}\times\mathbf{l}\rangle .$$

These quantities do not in general separate:

$$\langle \mathbf{l}\times\mathbf{s}\rangle \neq \langle \mathbf{l}\rangle\times\langle \mathbf{s}\rangle ,$$

$$\frac{1}{i\hbar}\langle [\mathbf{l},h_{el}(l_z;R)]\rangle \neq \langle \mathbf{G}(l_z;\mathbf{R})\rangle\times\langle \mathbf{l}\rangle . \tag{4.14}$$

Because of this, the exact evolution of quantum expectation values cannot be described by a closed set of equations like (4.9). Therefore, the quantum evolution of $\langle \mathbf{l}\rangle$ and $\langle \mathbf{s}\rangle$ must differ in some ways from the classical evolution of $\bar{\mathbf{l}}(t)$ and $\bar{\mathbf{s}}(t)$.

By comparing quantum calculations (such as those described in Sec. III) with the predictions of the quasiclassical equations of motion (4.9), we have identified the following differences between quantum and quasiclassical behavior.

Electrostatic coupling: (1) The classical $\bar{\mathbf{l}}(t)$ precesses in a circle about the internuclear axis; however, the quantum $\langle \mathbf{l}(t)\rangle$ may trace out a circle or an ellipse.

(2) The frequency of precession of the classical $\bar{\mathbf{l}}(t)$ is proportional to $\bar{l}_z$; hence this frequency depends upon the initial conditions. However, the frequency of precession of the quantum $\langle \mathbf{l}(t)\rangle$ is fixed and equal to $|\epsilon_\Sigma - \epsilon_\Pi|/2\pi\hbar$, independent of initial conditions.

(3) If initially the classical $\bar{\mathbf{l}}(t_0)$ is perpendicular to the internuclear axis, then $d\bar{\mathbf{l}}(t)/dt = 0$, and $\bar{\mathbf{l}}(t)$ is fixed; there is no precession. Similarly, the quantum $\langle \mathbf{l}(t)\rangle$ does not precess—instead it oscillates at the same frequency (the ellipse traced out by $\langle \mathbf{l}(t)\rangle$ degenerates to a straight line).

Spin–orbit coupling: (4) Quasiclassical $\bar{\mathbf{l}}$ and $\bar{\mathbf{s}}$ precess in circular cones centered on their resultant $\bar{\mathbf{j}}$; however, quantum $\langle \mathbf{l}\rangle$ and $\langle \mathbf{s}\rangle$ trace out elliptical cones that are not exactly centered on their resultant $\langle \mathbf{j}\rangle$. In either case, $\bar{\mathbf{j}}$ or $\langle \mathbf{j}\rangle$ is exactly conserved.

We did not find any other important qualitative differences between quantum and classical behavior. In particular we can prove that when $\langle l_z\rangle \neq 0$, the classical equations of motion give the correct sense of precession (Appendix). With these reservations, the classical equations of motion provide an intuitive understanding of the evolution of the quantum expectation values.

V. POLARIZATION EFFECTS

We now use the theory described above to calculate experimentally measurable total cross sections and alignment effects for Na fine-structure transitions from the $j = 3/2$ level to the $j = 1/2$ level induced by collisions with He. Initial conditions are chosen to correspond to those prepared by a linearly polarized laser, and individual trajectory results are averaged over impact parameter. We note that although Na has hyperfine interaction[38] (the nuclear spin, I, is 3/2), its effect is negligible on the time scale of the collision, and thus we do not include the hyperfine term in the Hamiltonian; however, the hyperfine interaction does affect the initial conditions prepared by the laser.

Section V is organized as follows. In Sec. V A we calculate the alignment effect for the hypothetical case of Na with no hyperfine structure; we compare the result of this calculation with that of a full quantum treatment presented in the accompanying paper. In Sec. V B we repeat the calculation of the alignment effect, only now we include the hyperfine structure of the initial state. One might expect this to diminish any alignment effect; however, there is a pumping scheme using a continuous laser in which the alignment effect is just as large. Our treatment is specific to the system under discussion. A comprehensive tensor algebraic treatment of the effect of hyperfine structure on alignment cross sections is given in Anderson, Gallagher, and Hertel.[39] Finally, in Sec. V C we examine the effect of orbital locking on the preservation of the *initially prepared* collision alignment.

A. Alignment effect neglecting Na hyperfine structure

We consider the case of exciting ground state Na from the $^2S_{1/2}$ level to the $^2P_{3/2}$ level with a linearly polarized laser beam which propagates perpendicular to the plane defined by the crossed atomic beams. The total cross section for subsequent collisionally induced transitions to the $^2P_{1/2}$ level is to be measured as a function of laser alignment. In this section, we temporarily neglect the hyperfine structure.

The initial relative coordinate vector $\mathbf{R}(t = -\infty)$ and relative velocity $\mathbf{v}(t = -\infty)$ define the initial collision plane. (The nuclear trajectory is only slightly deflected out of this plane.[40]) For the purposes of this calculation, it is most convenient to define this to be the space-fixed $x'z'$ plane. (As always, the z' axis is the initial direction of motion of Na relative to He, $\mathbf{v}$.)

The electric field of the laser defines a line in space; the direction of that line is defined relative to the space-fixed frame by two angles (Θ_E,ϕ_E).

Before laser excitation, the Na atom is in a $3s$ state with a statistical mixture of $m_s = \pm 1/2$. We first treat the case where $m_s = +1/2$. If the laser polarization is parallel to the space-fixed z' axis ($\Theta_E = 0$), then, from familiar selection rules, the laser excites the atom to the state:

$$|i_{z'}\rangle = |3/2,1/2\rangle e^{i\delta} ,$$

where the ket is labeled by quantum numbers $|j,m_j\rangle$ and δ is an indeterminate phase. Similarly, if the laser polarization is aligned along the x' (or y') axis, the initial state is:

$$|i_{x'}\rangle = [-(3/4)^{1/2}|3/2,3/2\rangle + (1/4)^{1/2}|3/2,-1/2\rangle]e^{i\delta} ,$$

$$|i_y\rangle = [(3/4)^{1/2}|3/2,3/2\rangle + (1/4)^{1/2}|3/2,-1/2\rangle]e^{i\delta}.$$

An arbitrary alignment of the laser gives the initial state:

$$|i_{\Theta_E,\phi_E}\rangle = [\cos(\Theta_E)|i_{z'}\rangle + \sin(\Theta_E)\{\cos(\phi_E)|i_{x'}\rangle + \sin(\phi_E)|i_{y'}\rangle\}]e^{i\delta}.$$

As a result of collision, any intial state, $|i\rangle$, is carried into a corresponding final state, $|f\rangle$, and the probability of ending up in the $j=1/2$ level is:

$$P(b) = |\langle 1/2,+1/2|f\rangle|^2 + |\langle 1/2,-1/2|f\rangle|^2. \quad (5.1)$$

Obviously this transition probability depends on the laser polarization, and we denote it $P(b;\Theta_E,\phi_E)$.

The distribution of impact parameters is cylindrically symmetric about the average initial relative velocity vector **v**. Therefore, to calculate the experimentally measurable alignment cross sections, $\sigma_\parallel$ and $\sigma_\perp$, we must incoherently average the probabilities, $P(b;\Theta_E,\phi_E)$, over the azimuthal angle, ϕ_E, for each impact parameter, b. For the case of parallel laser polarization,

$$\sigma_\parallel = \int_0^{2\pi} d\phi_E \int_0^\infty db\,[bP(b;\theta_E=0,\phi_E)].$$

Since $P(b;\Theta_E=0,\phi_E)$ is independent of ϕ_E, we can write this as

$$\sigma_\parallel = \int_0^\infty db\,[2\pi bP(b;\Theta_E=0)]. \quad (5.2a)$$

For the case of perpendicular polarization, the average over ϕ_E gives

$$\sigma_\perp = \int_0^\infty db\,\pi b\,[P(b;\Theta_E=\pi/2,\phi_E=0) + P(b;\Theta_E=\pi/2,\phi_E=\pi/2)]. \quad (5.2b)$$

(The integral over b is summed numerically from $b=0.2$ to 20 bohr with steps of 0.2 bohr.)

Plots of each integrand as a function of impact parameter are given in Fig. 6. The oscillations shown in this figure should be experimentally observable if differential cross sections are measured. Minima corresond to trajectories where $\langle \mathbf{l}\rangle$ undergoes approximately an integral number of precessions.

The cross section for a given Θ_E is

$$\sigma_{\Theta_E} = \cos^2(\Theta_E)\sigma_\parallel + \sin^2(\Theta_E)\sigma_\perp. \quad (5.2c)$$

Similar formulas hold if the original Na spin state is $m_s = -1/2$, and the same cross section is obtained.

For Na $3p\,^2P_{3/2}$ colliding with He with a relative velocity of 9×10^{-4} a.u., we calculate by the above method:

$$\sigma_\parallel = 75 \text{ a.u.}^2,\ \sigma_\perp = 184 \text{ a.u.}^2,\ \sigma_\perp/\sigma_\parallel = 2.4.$$

This illustrates the substantial effect of laser polarization on the cross section for this hypothetical case.

At the time of this work there were no previous theoretical calculations nor experimental measurements of the alignment effect; a recent full quantum calculation (see accompanying paper) also predicts an alignment ratio of 2.4, in good agreement with our value of 2.5. As an additional check on our calculation we compute the degeneracy averaged total cross section and compare with previous theoretical and experimental results.

We do this both for the conditions above, where the relative velocity is 9×10^{-4} a.u., and for the conditions used in previous work, where the temperature is given as 400 K. [Temperature and average relative velocity are related by the expression $v = (8\,kT/\pi\mu)^{1/2}$.] Our results are:

$$\sigma_{tot} = 1/4 \sum_{m_j=-3/2}^{+3/2} \{\sigma_{3/2,m_j\to 1/2,1/2} + \sigma_{3/2,m_j\to 1/2,-1/2}\}$$
$$= 154 \text{ bohr}^2(43 \text{ Å}^2) \text{ for } T = 625 \text{ K}$$
$$= 148 \text{ bohr}^2(41 \text{ Å}^2) \text{ for } T = 400 \text{ K}.$$

This is in reasonable agreement with experiment[24] at 450 K, where although the cross section for $j=1/2\to3/2$ was measured, we can calculate the cross section for $j=3/2\to1/2$ by detailed balance, which gives ≈ 57 Å^2. From a similar semiclassical calculation at 400 K by Masnou-Seeuws and McCarroll[7] using a different potential, we again use detailed balance to calculate a cross section of 43 Å^2, while from a full quantum mechanical calculation at 400 K by Lemoine, Robbe, and Pouilly,[3] also using a different potential, we calculate by detailed balance a cross section of ≈ 50 Å^2.

B. Alignment effect for stationary pumping of Na

We now consider the experimental case of stationary pumping[23] of Na from the $^2S_{1/2}$, $F=2$ hyperfine level to the $^2P_{3/2}$, $F=3$ hyperfine level with a linearly polarized cw laser. Again, the cross section for collisional transitions to the $^2P_{1/2}$ level is to be measured as a function of alignment.

The "photon frame" (x'',y'',z'') is defined to have the z'' axis along the laser polarization vector, the y'' axis along the direction of laser propagation, and the x'' axis so as to complete a right-handed coordinate system. The laser pumps each of the five sublevels of the ground state $F=2$ level up to the corresponding $F=3$ sublevel (selection rule for linearly polarized light: $\Delta m_F'' = 0$). Each of these five upper sublevels can then spontaneously emit to two or three lower sublevels ($\Delta m_F'' = 0, \pm 1$). After about 15 such pumping cycles, the initial distribution over m_F'' states in the upper level is narrowed to the stationary pumping limit. For Na, the incoherent distribution of hyperfine states, $|F,m_F''\rangle$, and the corresponding probabilities $W_{m_F''}''$ are[23]

$$|3,3\rangle:|3,2\rangle:|3,1\rangle:|3,0\rangle:|3,-1\rangle:|3,-2\rangle:|3,-3\rangle = 0:\tfrac{1}{42}:\tfrac{10}{42}:\tfrac{20}{42}:\tfrac{10}{42}:\tfrac{1}{42}:0.$$

The measured cross section is then a weighted average of $|F,m_F''\rangle$ state cross sections:

$$\sigma = \sum_{m_F''} W_{m_F''}\sigma_{m_F''}. \quad (5.3)$$

Each hyperfine state, $|F,m_F''\rangle$, can be reexpressed in terms of states, $|F,m_F'\rangle$, defined with respect to the collision frame (x',y',z') axes, using rotation matrices[31] (the photon and collision frames are related by the Euler angles Θ_E and ϕ_E) with each $|F,m_F'\rangle$ state a coherent superposition of $|j,I,m_j',m_I'\rangle$ states. Thus, $|F,m_F''\rangle$ can be written as

$$|F,m''_F\rangle = \sum_{m'_I}\sum_{m'_j}\sum_{m'_F} e^{im'_F\phi_E} d^F_{m'_F,m''_F}(\Theta_E)\langle m'_j,m'_I|F,m'_F\rangle |m'_j,m'_I\rangle$$

$$= \sum_{m'_I} |F,m''_F,m'_I\rangle\,, \tag{5.4}$$

where the second relation defines the states $|F,m''_F,m'_I\rangle$ and I is the quantum number for nuclear spin ($I = 3/2$ for Na). The quantum numbers I and j are suppressed since they are constant ($j = 3/2$ for this $F = 3$ level).

For this particular system, the hyperfine interaction term is neglected in the electronic Hamiltonian. As a result, each $|m'_I\rangle$ state is decoupled from the dynamics of the collision process, and so remains space-fixed over the duration of the collision. In this special case, $|F,m''_F\rangle$ is an *incoherent* mixture of pure states $|F,m''_F,m'_I\rangle$, so that the cross section for each $|F,m''_F\rangle$ state is the sum of the cross sections $\sigma_{m''_F,m'_I}$ for each of these $|F,m''_F,m'_I\rangle$ states,

$$\sigma_{m''_F} = \sum_{m'_I} \sigma_{m''_F,m'_I}\,. \tag{5.5}$$

Evaluating Eqs. (5.1)–(5.2) for the state $|F,m''_F,m'_I\rangle$, we obtain the cross section:

$$\sigma_{m''_F,m'_I} = \sum_{m'_j}\sum_{m'_F} \left[d^F_{m'_F,m''_F}(\Theta_E)\right]^2 |\langle m'_j,m'_I|F,m'_F\rangle|^2 \sigma_{m'_j}\,, \tag{5.6}$$

a weighted average of the cross sections $\sigma_{m'_j}$ for different $|m'_j,m'_I\rangle$ states. Note that in this expression, $\sigma_{m'_j}$ is independent of m'_I since as previously mentioned $|m'_I\rangle$ is decoupled from the dynamics of the collision process. The cross sections $\sigma_{m'_j}$ are calculated by the method described in Sec. V A; we find that $\sigma_{3/2} = \sigma_{-3/2} = 232$ a.u. and $\sigma_{1/2} = \sigma_{-1/2} = 75$ a.u. Substitution of Eqs. (5.6) and (5.5) into (5.3) gives the measured cross section as a function of alignment:

$$\sigma(\Theta_E) = \sum_{m'_j}\left\{\sum_{m''_F} W_{m''_F}\sum_{m'_F}\left[d^F_{m'_F,m''_F}(\Theta_E)\right]^2 \times \sum_{m'_I} |\langle m'_j,m'_I|F,m'_F\rangle|^2\right\}\sigma_{m'_j}\,. \tag{5.7}$$

For a more general, comprehensive treatment of initial state preparation including hyperfine structure using a tensor analysis of the density matrix, see Appendices A–D of Anderson, Gallagher, and Hertel.[39]

The alignment selected cross sections [$\sigma_\parallel = \sigma(0°)$; $\sigma_\perp = \sigma(90°)$] and alignment effect are computed from Eq. (5.7) and are found to be

$$\sigma_\parallel = 101 \text{ a.u.}^2\,,$$

$$\sigma_\perp = 180 \text{ a.u.}^2\,,$$

$$\sigma_\perp/\sigma_\parallel = 1.8\,.$$

This illustrates the substantial effect of laser polarization on the cross section, despite the initial preparation of a mixture of hyperfine states.

C. Alignment preservation and orbital locking

Preparation of the initial Na $^2P_{3/2}$ state with the laser polarization vector parallel to the inital relative velocity vector results in an asymptotic Σ molecular state while perpendicular laser polarization results in an asymptotic Π molecular state.[41] Is the initially prepared asymptotic molecular alignment preserved as the atoms approach each other? In other words, if the asymptotic molecular state is Σ, does it remain Σ? This depends on the impact parameter. Take the case of laser polarization parallel to the initial relative velocity vector. If $b = 0$, clearly the orbital will remain parallel to the internuclear axis all the way into the distance of closest approach, and thus the system can be described as a Σ molecular state throughout the collision. However, if b is large enough so that the Na atom does not interact with the He, then the orbital stays space-fixed so that it will be aligned perpendicular to the internuclear axis at the distance of closest approach, thus becoming a Π molecular state. For other values of b an intermediate behavior is found.

Figure 7 shows the behavior of $\langle\lambda\rangle = \langle l_z/\hbar\rangle$, the expectation value of the projection of $\mathbf{l}$ onto the internuclear axis, over the course of various trajectories differing in impact parameter. The initial state in this case[42] is $|j = 3/2, m_j = -3/2\rangle$, where the axis of quantization is along the initial relative velocity vector. Well before the collision, since $\lambda = -m_l$ asymptotically, $\langle\lambda\rangle$ remains essentially constant. As the atoms approach each other, the internuclear axis rotates while $\langle m_l\rangle$ remains constant, resulting in a change in $\langle\lambda\rangle$. Finally, orbital locking occurs when the anisotropy of the potential overwhelms the angular coupling; $\langle\mathbf{l}\rangle$ precesses rapidly about the internuclear axis, conserving $\langle\lambda\rangle$ and thus the orbital alignment in the molecular frame. Orbital locking is seen to occur in all the cases shown in Fig. 7; however, the molecular alignment of the locked orbital depends upon b. The smaller the value of b, the more the initial molecular alignment is preserved.

Finally, we point out that although the asymptotic alignment with respect to the molecular axis is not preserved

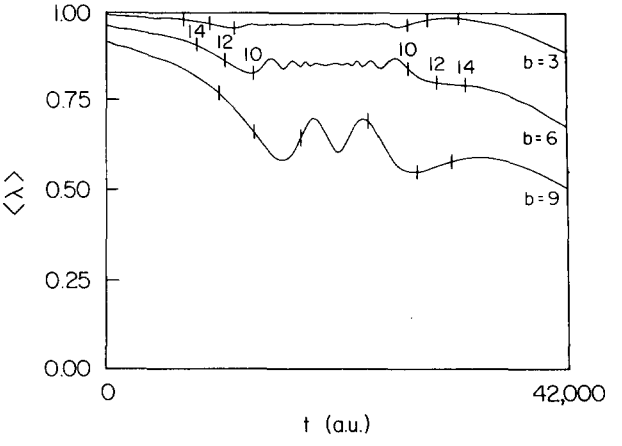

FIG. 7. Behavior of $\langle\lambda\rangle = \langle l_z\rangle/\hbar$ vs. time for the initial $|j = 3/2, m'_j = -3/2\rangle$ state over the course of three trajectories differing in impact parameter. A few corresponding values of R are indicated for each trajectory by the tick marks. Well before the collision (not shown) $\langle\lambda\rangle$ is constant; as the internuclear axis rotates, $\langle l'_z\rangle$ (the expectation value of the projection of $\mathbf{l}$ onto the space-fixed z' axis) remains constant while $\langle\lambda\rangle$ changes. When the locking radius is reached $\langle\mathbf{l}\rangle$ precesses rapidly about the internuclear axis as it rotates, thus conserving $\langle\lambda\rangle$. The sequence is reversed on the way out. Note how the value of $\langle\lambda\rangle$ within the locking radius differs with impact parameter.

for large impact parameter collisions ($b > 10$), there is still alignment specific dynamics, as seen from the large alignment effect in Fig. 6. The important point to consider is that for these large impact parameters, as b increases the retention of orbital alignment with respect to a *space-fixed* axis increases. Thus even at large impact parameters, the system prepared with parallel laser polarization is very different from that prepared with perpendicular laser polarization.

VI. CONCLUSION

We have obtained a picture of the mechanism for fine-structure transitions induced by collision. Figures 4(a)–(c) show how expectation values $\langle \mathbf{l} \rangle$ and $\langle \mathbf{s} \rangle$ change with time under various conditions. For the case of $Na^*(3p) + He$ collisions, the spin remains approximately space fixed, and the orbital angular momentum "locks" onto the internuclear axis at a radius $R \sim 14\, a_0$. Here "locking" means that $\langle \mathbf{l} \rangle$ precesses rapidly about the slowly rotating axis. The change of orientation of $\langle \mathbf{l} \rangle$ relative to $\langle \mathbf{s} \rangle$ results in a change of $\langle \mathbf{j} \rangle$, i.e., a fine-structure transition. For small enough impact parameters, orbital locking results in preservation of the initially prepared molecular alignment of the p orbital.

In hindsight, this intuitive picture is quite obvious, and it certainly would have been obvious to the Old Masters who studied molecular structure in the 1930's. For example, Herzberg's[12] Figs. 95–105 have some similarity to our Figs. 4(a)–(c). It seems, however, that today Herzberg's figures are often regarded as metaphorical representations of certain quantum coupling schemes (pictures that remind us to combine certain simple products of angular-momentum functions into various sorts of total-angular-momentum eigenfunctions). Our pictures are not metaphorical representations. Insofar as the theory discussed in Sec. II describes the collision, we can say that the precession and locking of $\langle \mathbf{l} \rangle$ and/or $\langle \mathbf{s} \rangle$ to the internuclear axis are real physical processes, which are observable in principle, and perhaps even observable in practice.

Finally, we have predicted an experimentally measurable alignment ratio for this process: for stationary pumping of the $F = 3$ hyperfine level with a linearly polarized laser, $\sigma_\perp / \sigma_\parallel = 1.8$.

ACKNOWLEDGMENTS

This research was supported by the National Science Foundation, the Jeffress Foundation, and the Office of Naval Research. JBD also acknowledges the hospitality of the Joint Institute for Laboratory Astrophysics during his Visiting Fellowship. We thank George S. Schatz for comments on the manuscript and S. V. ONeil for many helpful conversations. The computations were done on the JILA VAX 8600.

APPENDIX: SENSE OF PRECESSION OF $\langle \mathbf{l}(t) \rangle$

We consider the precessional motion of the expectation value of the quantum angular momentum about the internuclear axis induced by the electrostatic Hamiltonian. Holding the nuclei fixed, we define α to be the azimuthal angle of the angular momentum relative to the internuclear axis

$$\alpha = \tan^{-1}[\langle l_y \rangle / \langle l_x \rangle] . \tag{A1}$$

The electrostatic interaction causes this angle to change with time such that

$$\operatorname{sgn}\left(\frac{d\alpha}{dt}\right) = \operatorname{sgn}[(\epsilon_\Pi - \epsilon_\Sigma)\langle l_z \rangle] . \tag{A2}$$

This precession is in the same sense as that predicted by the quasiclassical equations.

Proof: Since we are considering only the electrostatic part of the Hamiltonian, without spin–orbit coupling, we may ignore spin entirely. Then the system wave function can be written in the form

$$\Psi = c_+ e^{-i\epsilon_\Pi t}\Psi_{\Pi +} + c_0 e^{-i\epsilon_\Sigma t}\Psi_\Sigma + c_- e^{-i\epsilon_\Pi t}\Psi_{\Pi -} \tag{A3}$$

where $c_\pm$ and c_0 are complex constants determined from the initial conditions.

Since these functions are eigenfunctions of l_z with eigenvalues $\pm 1, 0$, we find directly that

$$\langle l_z \rangle = (|c_+|^2 - |c_-|^2)\hbar . \tag{A4}$$

Similarly, using the approximation (2.9), together with the familliar angular-momentum ladder operations, we find that

$$\langle l_x \rangle = \left(\frac{\hbar}{\sqrt{2}}\right)[c_0(c_+^* + c_-^*)e^{i(\epsilon_\Pi - \epsilon_\Sigma)t} + \text{c.c.}]$$
$$\langle l_y \rangle = \left(\frac{\hbar}{i\sqrt{2}}\right)[c_0(c_+^* - c_-^*)e^{i(\epsilon_\Pi - \epsilon_\Sigma)t} - \text{c.c.}] . \tag{A5}$$

Now

$$\frac{d\alpha}{dt} = \left[\langle l_x \rangle \frac{d}{dt}\langle l_y \rangle - \langle l_y \rangle \frac{d}{dt}\langle l_x \rangle\right] \Big/ (\langle l_x \rangle^2 + \langle l_y \rangle^2) . \tag{A6}$$

Using (A5), we find that this is

$$\frac{d\alpha}{dt} = \frac{2\hbar|c_0|^2(|c_+|^2 - |c_-|^2)(\epsilon_\Pi - \epsilon_\Sigma)}{\langle l_x \rangle^2 + \langle l_y \rangle^2} \tag{A7}$$

$$= \left[\frac{2|c_0|^2}{\langle l_x \rangle^2 + \langle l_y \rangle^2}\right]\langle l_z \rangle(\epsilon_\Pi - \epsilon_\Sigma) . \tag{A8}$$

The first factor is positive, so Eq. (A2) is proved.

[1] R. H. G. Reid, J. Phys. B **6**, 2018 (1973).
[2] J. Pascale and R. E. Olson, J. Chem. Phys. **64**, 3538 (1976).
[3] D. Lemoine, J. M. Robbe, and B. Pouilly, J. Phys. B **21**, 1007 (1988).
[4] E. E. Nikitin, J. Chem. Phys. **43**, 744 (1965).
[5] F. Masnou-Seeuws, J. Phys. B **3**, 1437 (1970).
[6] F. Masnou-Seeuws and E. Roueff, Chem. Phys. Lett. **16**, 593 (1972).
[7] F. Masnou-Seeuws and R. McCarroll, J. Phys. B **7**, 2230 (1974).
[8] H. Schmidt, A. Bähring, and R. Witte, Z. Phys. D **1**, 71 (1986).
[9] J. Pascale, Technical Report, Service de Physique des Atoms et des Surfaces (C.E.N. Saclay).
[10] J. Grosser, J. Phys. B **14**, 1449 (1981); Z. Phys. D **3**, 39 (1986).
[11] I. V. Hertel, H. Schmidt, A. Bähring, and E. Meyer, Rep. Prog. Phys. **48**, 375 (1985).
[12] G. Herzberg, *Molecular Spectra and Molecular Structure* (Van Nostrand Reinhold, New York, 1950), 2nd Ed., Vol. 1, Chap. V, pp. 212–226.
[13] B. Pouilly and M. H. Alexander, J. Chem. Phys. **86**, 4790 (1987).
[14] G. C. Schatz, L. J. Kovalenko, and S. R. Leone, J. Chem. Phys. **91**, 6961 (1989).
[15] M. O. Hale and S. R. Leone, J. Chem. Phys. **79**, 3352 (1983); M. O. Hale, I. V. Hertel, and S. R. Leone, Phys. Rev. Lett. **53**, 2296 (1984); W. Bussert, D. Neuschäfer, and S. R. Leone, J. Chem. Phys. **87**, 3833 (1987).

[16]W. Bussert and S. R. Leone, Chem. Phys. Lett. **138**, 276 (1987); L. J. Kovalenko, R. L. Robinson, and S. R. Leone, Faraday Trans. 2, J. Chem. Soc. **85**, 939 (1989).
[17]M. P. I. Manders, J. P. J. Driessen, H. C. W. Beijerinck, and B. F. Verhaar, Phys. Rev. Lett. **57**, 1577 (1986); *ibid.* **57**, 2472 (1986); M. P. I. Manders, W. M. Ruyten, F. v.d. Beucken, J. P. J. Driessen, W. J. T. Veugelers, P. H. Kramer, E. J. D. Vredenbreght, W. B. M. van Hoek, G. J. Sandker, H. C. W. Beijerinck, and B. J. Verhaar, J. Chem. Phys. **89**, 4777 (1988).
[18]A. Z. Devdariani and A. L. Zagrebin, Chem. Phys. Lett. **131**, 197 (1986); A. Z. Devdariani and Yu. N. Sebyakin, Opt. Spectrosc. (USSR) **62**, 149 (1987).
[19]M. H. Alexander and B. Pouilly, in *Selectivity in Chemical Reactions*, edited by J. C. Whitehead (D. Reidel, Boston, 1988), p. 265; J. Chem. Phys. **90**, 5373 (1989); B. Pouilly, J. M. Robbe, and M. H. Alexander, J. Chem. Phys. **91**, 1658 (1989).
[20]M. P. I. Manders, J. P. J. Driessen, H. C. W. Beijerinck, and B. J. Verhaar, Phys. Rev. A **37**, 3237 (1988).
[21]P. I. Manders, W. B. M. van Hoek, E. J. D. Vredenbreght, G. J. Sandker, H. C. W. Beijerinck, and B. J. Verhaar, Phys. Rev. A **39**, 4467 (1989).
[22]E. E. B. Campbell, H. Schmidt, and I. V. Hertel, Adv. Chem. Phys. **72**, 37 (1988).
[23]I. V. Hertel and W. Stoll, J. Appl. Phys. **47**, 214 (1976); A. Fischer and I. V. Hertel, Z. Phys. A **304**, 103 (1982).
[24]J.-C. Gay and W. B. Schneider, Z. Phys. A **278**, 211 (1976).
[25]We note that since the electron coordinate is referred to the Na^+, which is not necessarily moving at constant velocity, the frame of reference is not an inertial frame. However the effects of acceleration of the frame of reference are believed to be negligible for this system. (In contrast, the effects of rotation of the basis functions are very important.)
[26]E. U. Condon and G. H. Shortley, *The Theory of Atomic Spectra* (Cambridge Univ. Press, New York, 1964).
[27]J. B. Delos, Rev. Mod. Phys. **53**, 287 (1981).
[28]Electron-translation factors can be ignored in this system, because the electron is always firmly situated on the Na atom, and there is no real or even virtual charge-exchange (see Ref. 27).
[29]For all $R \leqslant 18 \epsilon_\Sigma > \epsilon_\Pi$, but at $18 \leqslant R \leqslant 40$, his computed ϵ_Σ is very slightly less than ϵ_Π. This latter splitting is not discernible from Pascale's points shown in Fig. 1. We ignored this splitting in our fitted potentials because it is relatively small ($< 1.2 \times 10^{-2} \times$ soc) and happens at such large distances; for the present case it has little effect on cross sections.
[30]C. E. Moore, *Atomic Energy Levels*, National Standard Reference Data Series-NBS 35 (1971); S. Bashkin and J. O. Stoner, Jr., *Atomic Energy Levels and Grotrian Diagrams* (Elsevier, New York, 1975).
[31]Particle Data Group, Rev. Mod. Phys. **48**, 536 (1976); R. N. Zare, in *Angular Momentum* (Wiley, New York, 1988), pp. 85–91.
[32]J. B. Delos, W. R. Thorson, and S. K. Knudson, Phys. Rev. A **6**, 709 (1972).
[33]Note that $\nabla \mathbf{h}$ is the matrix of the gradient of h, not the graident of the matrix of h.
[34]Energy conservation permits reduction of (2.19a) and (2.19b) to a single first-order differential equation, so that only three equations determine the nuclear trajectory. However, we found the pair of equations (2.19a) and (2.19b) to be more convenient for numerical integration.
[35]The basis functions rotate with the internuclear axis, but the angular coupling terms cause the coefficients $c(t)$ to change with time such that the actual electronic state Ψ stays exactly space-fixed.
[36]The point here is that the Born–Oppenheimer eigenvalues and the spin-orbit effects are calculable by standard methods of quantum chemistry. Our philosophy is that when we can use such "static" (fixed R) information as input to a calculation of the dynamics of a collision.
[37]A similar treatment is presented by H.-D. Meyer and W. H. Miller, J. Chem. Phys. **70**, 3214 (1979).
[38]E. Arimondo, M. Inguscio, and P. Violino, Rev. Mod. Phys. **49**, 31 (1977).
[39]N. Andersen, J. W. Gallagher, and I. V. Hertel, Phys. Rep. **165**, 1 (1988).
[40]Conservation of total angular momentum requires any change in electronic angular momentum, **j**, to be compensated for by a change in the nuclear orbital angular momentum, **N**.
[41]Due to the spin orbit coupling of the ^2P state of Na, a linearly polarized laser cannot prepare a pure Π or Σ molecular alignment of the p-orbital. (It can however do so for the case of excitation to the ^1P state of Ca.) Parallel polarization prepares 67% Σ while perpendicular polarization prepares 85% Π.
[42]For the sake of clarity, we use as initial state the $|j = 3/2, m_j = -3/2\rangle$ state of Na, which corresponds to a pure Π molecular state and can be prepared by using a circularly polarized laser propagating along the initial relative velocity vector.